IEEE Access
Multidisciplinary ⋮ Rapid Review ⋮ Open Access Journal

Received 17 September 2024, accepted 30 September 2024. Date of publication 00 xxxx 0000, date of current version 00 xxxx 0000.

Digital Object Identifier 10.1109/ACCESS.2024.3474089

Remaining Useful Life Estimation of Used Li-Ion Cells With Deep Learning Algorithms Without First Life Information

I. SANZ-GORRACHATEGUI[1], Y. WANG[2], (Senior Member, IEEE), A. GUILLÉN-ASENSIO[1], A. BONO-NUEZ[1], B. MARTÍN-DEL-BRÍO[1], (Senior Member, IEEE), P. V. ORLIK[2], (Senior Member, IEEE), AND P. PASTOR-FLORES[1]

[1]Department of Electronics and Communications Engineering, University of Zaragoza, 50018 Zaragoza, Spain
[2]Mitsubishi Electric Research Laboratories, Cambridge, MA 02139, USA

Corresponding author: A. Bono-Nuez (antoniob@unizar.es)

This work was supported in part by the Fulbright Commission, in part by the Estrategia Aragonesa de Especialización Inteligente en Investigación e Innovación (RIS3) Aragon Government through the EU Project Sistemas de Almacenamiento Híbridos e Inteligentes (SAHI) (LMP16 18), in part by the Catedra Sociedad Ibérica de Construcciones Eléctricas (SICE) (SICE Chair) of the University of Zaragoza, and in part by the Industrial Doctorate Program of the University of Zaragoza under Grant DI 6/2020.

ABSTRACT The second life use of lithium-ion batteries has gained significant attention in recent years, driven by the potential to repurpose cells from electric vehicles for less demanding applications. A critical aspect of this repurposing is accurately estimating the Remaining Useful Life (RUL) of the batteries. Traditional techniques often rely on data from the battery's first life, which may not be available in practical scenarios. To address this issue, we propose a data-driven method for RUL estimation that does not depend on first-life information. Our approach considers a realistic scenario where an aged battery cell, lacking previous usage data, is evaluated for second life use through a limited number of test cycles. We compute features such as incremental capacity curves, and other health indicators from the measured voltage and current waveforms of the used cell. These features are automatically processed by deep learning algorithms, including Convolutional Neural Networks (CNNs) and Long Short-Term Memory (LSTM) networks. This methodology achieves an average error of only 62 cycles for cells with a lifespan of up to 1200 cycles and a RUL error of less than 10% for deeply aged batteries. These results outperform state-of-the-art algorithms that utilize data from the cell's entire lifespan, demonstrating the efficacy and robustness of this approach.

INDEX TERMS Remaining useful life, second life battery, LFP, incremental capacity, deep learning, CNN, LSTM.

I. INTRODUCTION

Energy Storage Systems (ESS) based on lithium-ion batteries have become the standard for many different applications, mainly due to their high efficiency, energy and power density, and their declining manufacturing cost [1], [2]. Lithium-ion technologies such as LFP, NMC, LTO, or NCA provide longer service lives than other traditional alternatives, such as lead-acid, and are less contaminating than nickel related chemistries, such as NiCd [3], [4]. Thus, these lithium-ion technologies are the main option for Electric Vehicle (EV) applications [5], [6], [7], [8].

However, the expansion of the EV is generating a huge second-hand battery market, and reusing lithium-ion batteries in other applications, after their first life has expired, is a promising concept that has been studied from an economic, technical and environmental point of view [9], [10]. In this regard, low-demand applications in terms of instant power requirements and depth of discharge (DoD), are suitable second-life applications, as is the case with on-grid systems [9], [10], [11], [12]. In this field, the accurate estimation of the Remaining Useful Life (RUL) of the used cells remains

The associate editor coordinating the review of this manuscript and approving it for publication was Xinyu Du.

a key challenge to provide security and reliability to these systems.

The aging of lithium-ion batteries has been extensively studied, being a challenging problem [13], [14], [15], [16], [17], [18]. Traditionally, State of Health (SoH) has been the focus of these studies, although RUL is becoming more relevant in Energy Management System (EMS) strategies. These works are usually focused on real time applications, i.e., predict ESS failures [19], [20], [21], [22], [23], [24]. Furthermore, determining RUL for a second life application usually requires knowledge (data) on its first life use [25], [26].

Regarding the techniques used for RUL estimation, there are two traditional approaches to the problem: model-based and data-driven techniques. Model-based techniques are suitable for battery behavioral models (such as State of Charge estimators), but they have also been used for aging estimation [27], [28], [29]. However, due to the large number of factors involved in battery aging, highly accurate models are often difficult to develop.

For this reason, data-driven approaches can be an alternative [30], [31], [32], [33]. These methods present two main challenges. One of these challenges is the need for large datasets, which are difficult to obtain due to laboratory requirements. There are well-known publicly available datasets for certain chemistries [19], [34], [35], and even though they are small data-wise for the most recent deep learning techniques (hundreds of cells, thousands of cycles), some authors have used them successfully [36], [37]. As an alternative, some studies propose the use of synthetic datasets for training complex networks structures based on transformers [38].

The second challenge is the feature extraction and processing stages. Most studies rely on features that need to be tracked over cell life [36], [37] (e.g., capacity, internal resistance (IR)) to estimate the behavior of the cell in future use. In principle, this invalidates the use of data-driven techniques for applications where these variables cannot be obtained in-situ, or applications where the first life of the battery is unknown or there is no logged data from it.

In the well-known paper [35], Severson et al. introduce a dataset which contains information on 124 cells cycled under different charging conditions until their End of Life (EoL), defined as their capacity dropping below 80% of their nominal capacity. This dataset provides more than 90,000 full discharge cycles, with different measured features, such as voltage, capacity, or internal resistance. In the original paper, the authors use this dataset for RUL prediction, introducing some novel health indicators (HI). Their focus is the early RUL estimation of a monitored cell, before it shows capacity-fade. For this purpose, they explore several discrete features, obtained by pre-processing the data corresponding to the first 100 cycles of life.

In this work, the authors also hint at a different analysis that could be performed on the derivative of the discharge waveforms, also known as Incremental Capacity (IC) curves, which contain information on degradation. These curves have been previously described in [31], [39], [40], [41], [42], and their peaks have been proven to be a useful source of information to diagnose battery aging and the causes of degradation [38], [43], [44], [45].

However, in our opinion, there is still potential for applying an automatic data-driven analysis to these raw waveforms for RUL estimation, hence our approach will present two main constraints as novelties. On the one hand, the methodology introduced in this paper uses raw IC curves, without (manual) pre-processing, and deep learning models for automatic feature extraction. On the other hand, the main novelty of the proposed methodology is that it does not require data from the cell's first life. This generalization capability allows for its application in situations where historical data on the cell's first life is not available.

Thus, in the methodology proposed in this paper, a single cell is evaluated at an unspecified moment in its lifecycle to determine its potential for second-life applications. A limited number of test cycles are conducted to extract raw IC curves from the measured voltage and current waveforms of the cell, and additional features, such as capacity or internal resistance, are calculated. These features are then used by deep learning algorithms to estimate the cell's RUL, expressed as a function of its remaining Full Equivalent Cycles (FEC). In the scope of this paper, Convolutional Neural Networks (CNN) and Long Short-Term Memory (LSTM) are used as data-driven techniques to this end (notice that, although more recent sequence-processing techniques, such as transformers, could be used, they require huge datasets). Finally, multiple error metrics are calculated and compared to those achieved by current state-of-the-art algorithms applied to the same dataset. Unlike these traditional methods that rely on first life data of the cell, the presented methodology demonstrates better performance without requiring such information.

The paper is organized as follows. In Section II, the dataset is presented and our approach to RUL estimation is described. In Section III, the deep learning architectures used, and the methods to avoid overfitting applied, are shown. Section IV presents the results obtained with our methodology, including comparisons with other techniques. Finally, the conclusions are summarized in Section V.

II. METHODOLOGY

Conventional approaches to battery health estimation are model-based or make use of machine-learning techniques [23]. In this second approach, different features are manually extracted from the battery test cycles, and then they are used to train a machine learning algorithm that provides SoH or RUL estimation.

By using this second approach as a starting point, our study proposes the two main novelties indicated in Section I. First,

instead of selecting some features as inputs, raw IC waveforms are used as the main input to our algorithms (carrying out only minimal data preprocessing), thus providing as much information from each test cycle as possible (feature extraction used in other works often involves some information loss). Hence, the required machine learning model should be complex enough to handle whole waveforms. For comparison purposes, the algorithms developed in this study will be tested against other techniques that do involve feature extraction.

Second, when the RUL of a used cell is estimated for its possible use in the second life market, first life cell data is usually not available, but conventional techniques require tracking the evolution of the whole cell lifespan, thus they are not suitable in a realistic scenario. In this work, we develop a methodology that uses only local information corresponding to only a few test cycles, rather than the whole cell lifespan. In a real test scenario, when a used cell must be analyzed, first some test cycles are carried out and then these measurements are processed by a model trained for RUL estimation, providing the remaining FEC of the cell. With this information, it can be decided whether the cell is suitable for a second life application or not.

A. DATASET

The Toyota Research Institute provides the dataset used in this study. It was initially introduced in [35], and it has been used previously in other studies such as [46], [47]. It contains approximately 96,700 charge/discharge cycles from 124 commercial LFP/graphite cells, which allow us to extract thousands of training examples for training machine learning models. The specific model of the cell is APR18650M1A from A123 Systems, and its nominal capacity is 1.1Ah. The cells have been tested with high-current charge and discharge cycles, from the beginning of their life until the end. The life of the cells varies greatly in the dataset, ranging from a few hundred FEC to more than one thousand in some cases.

The charging current waveforms are not constant from cell to cell since their original purpose was to test different charging conditions. However, the discharge current for all cycles across all cells was indeed constant, at a 4C rate (4.4A). During the cycles, the ambient temperature was set to 30°C, although it increased along with the test duration due to self-heating. Voltage, current, and temperature waveforms were measured for each discharge. Additionally, the original authors provide a capacity and an internal resistance (IR) measurement for each cycle. Capacity is measured by integrating the charge obtained during the full-discharge process. IR is obtained by processing current pulses and their voltage response while charging.

The dataset is provided by the original authors in three different batches, with differences among them. For example, the second batch consists almost exclusively of cells with poor life performance, whereas the other batches are better in this sense.

As an initial hypothesis, each discharge waveform in the database has been considered as a single, independent test, uncorrelated to each other. Thus, the training, validation, and test subsets were randomly created by selecting cycles across the whole dataset. This will have further implications, which we will expand on in the next sections.

B. INPUT DATA AND FEATURE SELECTION

Traditional machine learning approaches usually need a previous feature extraction stage to extract key features from the data. In the case of battery aging estimation, common examples of such features are capacity or internal resistance. A health indicator that is gaining traction in recent years is Incremental Capacity (IC) [31], [39], [40], [41], [42]. IC curves are defined as the partial derivative curve of the charge q against the voltage v of the cell (1), for a specific cycle, with constant current.

$$IC\,(\upsilon) = \frac{\delta q(\upsilon)}{\delta \upsilon} \tag{1}$$

Thus, the IC curve can be obtained directly from the voltage waveforms contained in the dataset. The IC curves show different capacitance peaks at different voltage values, depending on each chemistry and aging process. These peaks are the regions of voltage where the cell stores energy, and vary slightly along the cell's life. The peaks and their variation have been proven to be good indicators of battery life and different degradation mechanisms, and they show great potential for SoH and RUL prognosis [37], [41].

One of the novelties in our study is to consider as much information as possible provided by the IC curves in the dataset, with minimal pre-processing. Since the discharge process in every cycle was made with the same nominal current, we opted for using the discharge IC waveforms as the inputs. An example of these cycles and their associated IC waveforms is shown in Fig. 1, where multiple cycles from the same cell are depicted, belonging to different moments of its life. Each plot in Fig. 1 represents a different test cycle, dark blue being the least aged cycle and cyan being the most aged cycle.

It must be observed that genuine IC waveforms are obtained with low charge and discharge rates on the cells (around 0.05C). This is not strictly the case in this dataset since the cells are discharged at 4C, but we will consider these curves as an approximation of the original IC curves. As it may be appreciated in Fig 1. (b), as the cell ages (cyan), a secondary IC peak appears in the range of 2.4V. This peak is a clear indicator of aging, and it is one of the target features for the deep-learning algorithm. When processing genuine IC curves, better results would be expected. Nevertheless, using high-rate curves in a real test scenario could be more convenient from an application perspective due to the reduced testing time, since testing at 4C is 80 times faster than at 0.05C.

Machine learning methods often benefit from (or sometimes even require) normalized input data; usually, every input is normalized to mean 0 and standard deviation 1. However, when normalizing IC curves, some absolute information

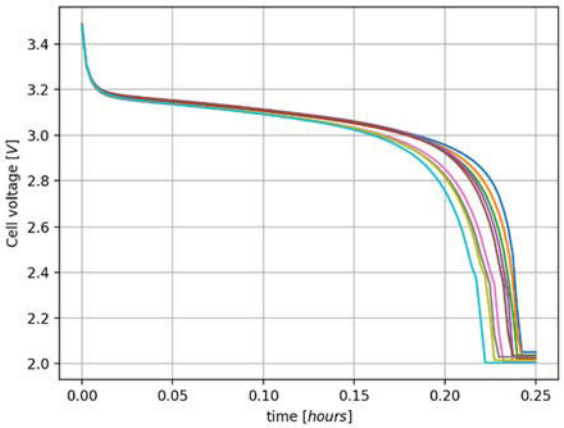

(a)

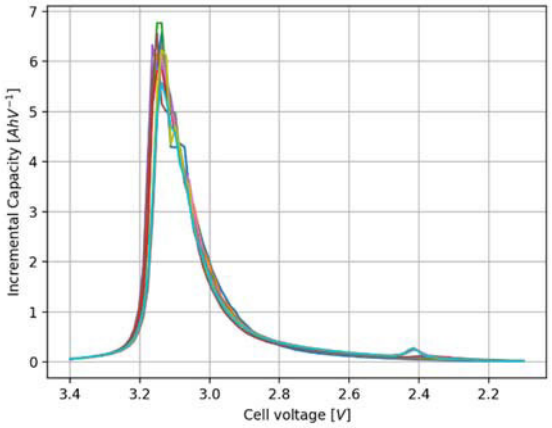

(b)

FIGURE 1. Time-domain voltage waveforms from a single cell along its lifespan (a). Incremental capacity waveforms belonging to the time-domain waveforms (b). Each plot represents a different test cycle of the same cell, with the cyan one being the latest cycle corresponding with the most aged situation and the dark blue one with the least aged situation. These colors can be easily distinguished at the tails of the discharge waveforms in (a).

may be lost, such as the area below the IC curve, which represents cell capacity. For this reason, some discrete features have also been considered as input data: capacity, IR, and Time Interval of Equal Discharging Voltage Difference (TIEDVD). As already introduced, capacity and IR obtention is detailed in [35]. TIEDVD is the time interval between two voltage thresholds (V_{max}, V_{min}). It can be obtained with minimal pre-processing from the discharge waveforms, and has proven to be a good health indicator in other studies [19], [22], [48], [49], [50]. In our previous work [48], it was found that the thresholds 3.3V and 3.15V show good estimation capabilities for this chemistry. These additional features and their evolution for one specific cell are shown in Fig. 2.

As stated before, one main novelty of our work is that the estimation approach does not rely on past information about the usage of the cell. By only performing a limited set of test cycles to the cell under study, the algorithm will estimate its RUL. Nevertheless, more than one test cycle will be performed to extract more information. In [48], it was established that ten test cycles provide a good trade-off between accuracy and model complexity. We use deep learning models capable of processing ten IC waveforms plus ten groups of additional input variables, which can handle temporal correlation between different test cycles.

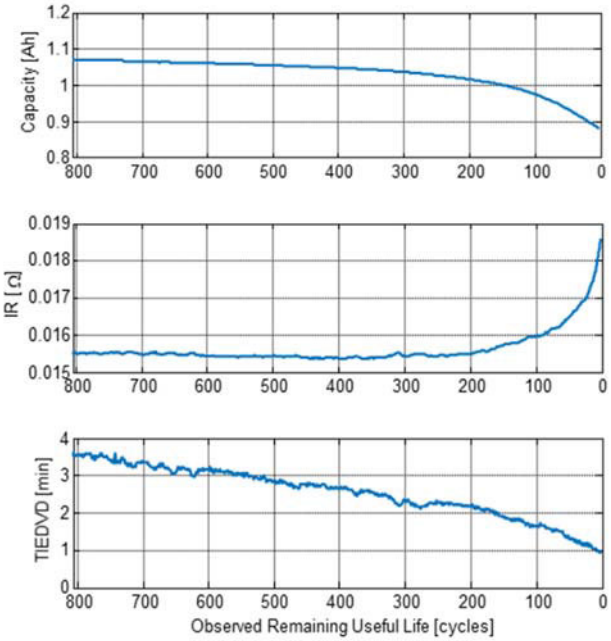

FIGURE 2. Capacity evolution for a sample cell (top). IR evolution for a sample cell (center). TIEDVD evolution for a sample cell (bottom).

III. DEEP LEARNING ALGORITHMS

A. DEEP LEARNING MODELS USED

As specified in the previous section, it is required a machine learning model capable of analyzing a set of raw IC waveforms (ten curves). Our dataset includes about 96,700 charge/discharge cycles, which has allowed us to arrange a set of 84,762 training examples. Thus, we have selected two well-known deep learning models that have high performance and can be trained by using a moderate sized dataset (thousands of examples): Convolutional Neural Networks and Long-Short Term Memory [51]. The performance achieved by both deep learning models will be compared with other machine learning models (Section IV). It is important to note that we have discarded state-of-the art deep learning models, such as transformers [52], because transformers include millions of parameters, requiring huge datasets (millions of examples).

1) CONVOLUTIONAL NEURAL NETWORKS (CNN)

CNNs are deep learning algorithms originally introduced for image processing [51]. CNNs are based on 2D convolutional filter layers that scan the input image for feature detection, interleaved with pooling layers for dimensionality reduction. Finally, some fully connected layers provide the output.

Although CNNs were introduced for image processing [51], CNNs can also process waveform signals. For instance, in [53] a CNN is applied to EEG (electroencephalographic) signals, constructing a 'virtual image' by grouping some EEG waveforms of the same length (vector data) forming a data matrix (a virtual image), where the X axis represents time and the Y axis, the signal values of several EEG waveforms. This allows the application of image processing techniques, such as convolutional networks, to a set of signal waveforms.

Thus, in our approach, the IC curves from ten measurement tests constitute a virtual image, which will be the input to a CNN that automatically extracts features from them. As the cycles in the dataset have a different length (and so do the IC curves), they have been re-sampled to 100 samples each. Thus, the virtual images formed with ten IC curves have a dimension of 10×100 (Fig. 3). In this case, the virtual images have voltage in the X axis and time in the Y axis, whereas IC values are in the Z axis, represented as blue levels in Fig. 3.

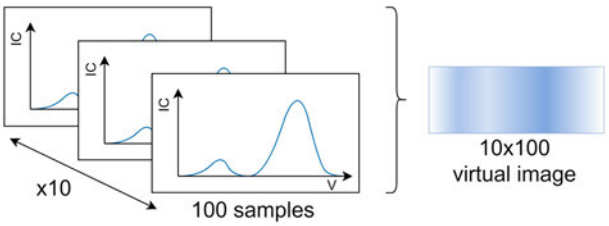

FIGURE 3. Ten incremental capacity waveforms grouped in a virtual image.

The CNN architecture proposed (Fig. 4) processes these 10×100 inputs by a set of four layers that automatically extract some key features: convolutional layer, average pooling layer, convolutional layer and average pooling layer. Then, two fully connected layers (Fig. 4) process the extracted features. Finally, an output neuron provides the RUL estimation in terms of remaining FEC. Other hyperparameters to be adjusted are the number of input and output channels, the shape of the convolutional and pooling kernels, and the stride hyperparameter. After several hyparameter searches, the best configuration found is shown in Table 1.

TABLE 1. Convolutional neural network configuration.

Layer	Type	Hyparameters
I	Convolutional layer	Channels in:1 out:2 Kernel 5x1 Stride 2x1
II	Average pooling	Kernel 2x2
III	Convolutional layer	Channels in:2 out:4 Kernel 1x5 Stride 1x2
IV	Average pooling	Kernel 1x2

After the convolutional and pooling layers stages (preprocessing network from now on), the algorithm reduces the input from $10 \times 100 = 1000$ values to four channels with shape 1×12 (Fig. 4). These extracted features are then unwrapped into a single array of 48 features, which needs to be post-processed to finally obtain the cell RUL. Several linear and nonlinear final layers with different number of neurons per layer were tried. The best results were obtained with two fully connected layers, with the number of neurons equal to the features to be processed, configuring a preliminary 48-48-48-1 feedforward network.

For the reasons explained in Section II-B, we also include as inputs some additional features, capacity, IR, and TIEDVD. These are introduced to the model after the pre-processing layer (Fig. 4), to be post-processed together with the 48 features that the convolutional layers extracted.

Thus, the complete deep network is shown in Fig. 4, where the neurons of the final fully connected layers have been adjusted to 78-78-78-1 to accommodate ten measurements of the three additional features, along with the 48 features extracted from the IC curves by the convolutional layers.

2) LONG SHORT-TERM MEMORY (LSTM)

Recurrent neural networks (RNN) are commonly used for processing temporal series [51]. Conventional RNN detect short-term features in a data series, but suffer from vanishing gradient problems, which leads them to forget long-term relationships. LSTM were proposed as a solution for detecting both short-term and long-term correlations [54] and are widely used for temporal data [51].

The structure of an LSTM cell is shown in Fig. 5. At any instant n, each cell has an input $\mathbf{x}^n$, an output $\mathbf{h}^n$, and a memory term $\mathbf{c}^n$, which change over time. Although indicated as scalar values, they can be vectors with p components. The LSTM cell controls information through three subnetworks, or ''gates'' (Fig. 5): forget gate $\mathbf{f}$, input gate $\mathbf{i}$, and output gate $\mathbf{o}$. The forget gate controls how much old information is removed from the memory term. The input gate controls how much new information in $\hat{\mathbf{c}}$ (main layer output) passes to the memory term. Finally, the output gate controls the impact the memory term has on the output $\mathbf{h}$. In Fig. 5, the σ and *tanh* blocks represent fully connected neural layers with sigmoid or hyperbolic tangent as activation functions, respectively.

Several LSTM cells can be concatenated so that the outputs of the previous serve as input to the following one, thus forming complex LSTM networks. Therefore, when designing these networks, two main hyperparameters must be adjusted: the dimensionality of the memory term p, and the number of LSTM cells concatenated.

In the case of our LSTM network for RUL estimation, the input $\mathbf{x}$ will be a sequence of ten IC waveforms. The same re-sampling indicated for the CNN has been applied to the waveforms, so each waveform will have 100 samples. When including the three additional features (capacity, IR, and TIEDVD), each element $\mathbf{x}^n$ in the sequence will include 103 features (100 samples belonging to the IC waveform, plus the three additional features). By executing several attempts, the best configuration found for the LSTM network for this problem is shown in Table 2.

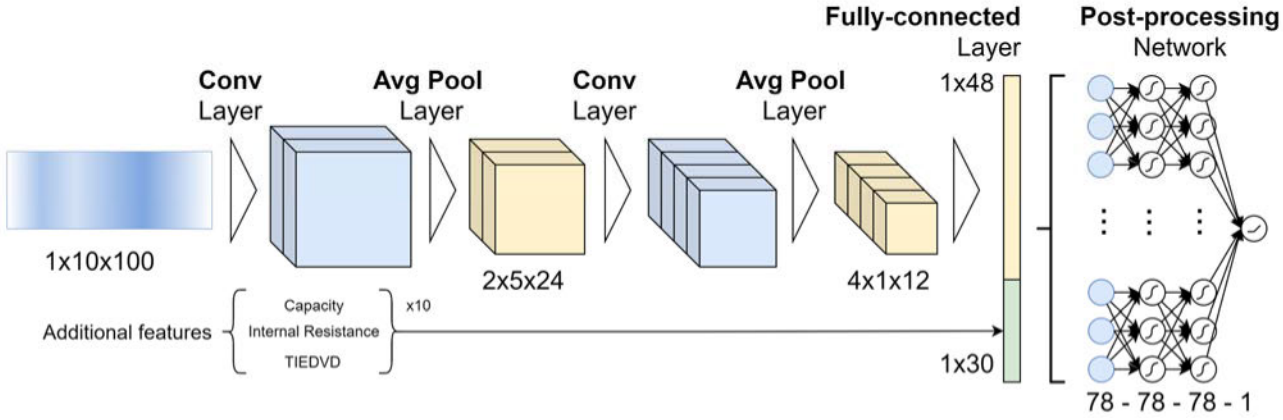

FIGURE 4. CNN architecture proposed: input virtual image (1 × 10×100), first and second convolutional and average pooling layers (AvgPool), and output fully connected layers (78-78-78-1).

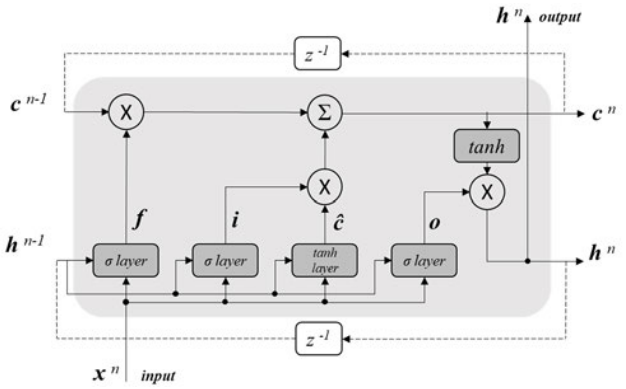

FIGURE 5. LSTM cell architecture.

TABLE 2. LSTM network configuration.

Hyperparameter	Value
p	25
Number of LSTM cells	2

B. OVERFITTING AVOIDANCE

Neural network models are prone to overfitting, especially with limited datasets, as is the case with battery datasets. To avoid this problem and ensure good generalization [51], [52], multiple regularization techniques have been used.

Early-stopping [51] is a classical regularization technique. It consists of dividing the dataset in three subsets: a training set (60%), for model learning; a validation set (20%), for monitoring the generalization error and stopping the training at the point of minimum validation error (maximizing generalization); and a test set (20%) used for the final evaluation of the model performance.

As explained in Section II-A, each training sample (comprised by data of 10 consecutive cell cycles) was initially considered as an individual sample, uncorrelated with the rest of the samples that originated from the same battery cell. The division into training, validation and test sets was done accordingly by randomly assigning each example to one of the three subsets (Fig. 6, a).

In our first test, the results of deep learning algorithms when applying early-stopping were impressive, achieving a root mean squared error (RMSE) when estimating RUL as low as 10 FEC. We suspected that these results were very optimistic, and we verified that the model was overfitting, which was unexpected, since early-stopping was being used. In this case, overfitting was occurring at a higher level, overfitting battery cells instead of data cycles. Even though information from different cycles was separated between the different subsets, the network learned how specific battery cells in the database behave and provided very good estimations for other examples belonging to the same battery cell. To solve this issue, we changed the initial way of dividing the three subsets (Fig. 6, a), and implemented a battery cell-based division (Fig. 6, b).

The cycles belonging to each individual cell are all assigned to one of the subsets. By dividing the data this way, no examples from the same battery cell are used across training, validation, and testing. This is also a more realistic approach considering the final application, since in a real case the cell under test will be unrelated to the training process, i.e., it will be a cell not used for building the model. After making this change in the subset creation, the model was trained again. By using early stopping with this subset division, the optimal network size and the rest of the hyperparameters (number of epochs, learning rate) were determined.

However, even though the dataset is comprised of many cycles, it only includes 124 battery cells. Dividing this dataset into three subsets ends up with a small number of battery cells in each subset. Thus, cross-validation techniques [51] have been applied for obtaining more realistic and comparable error estimation.

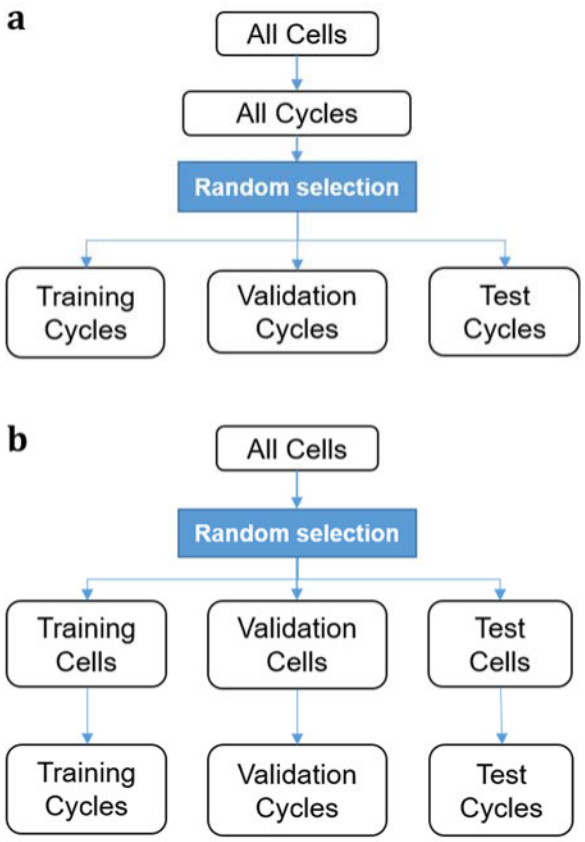

FIGURE 6. Old subset division, with overfitting at battery cell level (a). New subset division (b).

First, k-fold cross-validation (k-CV) was used [51]. It consists of dividing the initial dataset evenly into k sub-groups. In this application, $k = 10$ groups were selected, since it has been seen that this number provides a good trade-off between computing time and accuracy [55]. Then, the model is trained with 9 groups and validated with the 10th group. This process is repeated 10 times, in such a way that every group is used as validation set on one occasion. Numerical results achieved will be shown and discussed below.

Finally, as it is usual with small datasets, Leave-One-Out (LOO) cross-validation has also been used [51]. LOO is a special case of cross-validation in which $k = N$ (being N the number of examples). In this case, the net is trained N times by using N-1 battery cells for training and one cell for validating (on each training, a different cell is 'left out'). As shown in Sect. IV, standard tenfold cross-validation and LOO provide comparable results, although errors estimated by LOO are slightly better. The results obtained with this technique are the closest we could expect in a real application environment in which the whole dataset would be used for training.

Additionally, to avoid overfitting to a higher degree, different regularization methods were tried. These regularization methods include [51] Ridge regularization, Lasso regularization, and other techniques, such as dropout layers or adversarial training [56], [57].

Ridge (2) and Lasso (3) regularization include the weights of the network w_j into the loss function J, to penalize large weights and achieve smoother output functions:

$$J = \frac{1}{N}\sum_{i=0}^{N-1}(y - f(x_i))^2 + \lambda\sum_{j=0}^{P-1} w_j^2 \tag{2}$$

$$J = \frac{1}{N}\sum_{i=0}^{N-1}(y - f(x_i))^2 + \lambda\sum_{j=0}^{P-1} |w_j| \tag{3}$$

where J is the cost function (loss), N is the number of examples in the dataset, x_i is the i-th example in the dataset, y is the net output for that example, P is the number of weights in the network, w_j is the j-th weight and λ is a hyperparameter. The optimal λ value for both regularization techniques was found at 0.003 via a parametric sweep.

Dropout is another common methodology used to avoid overfitting [51]. Dropout layers are included after the hidden network layers and, in every training epoch, they randomly disconnect some neurons in these layers with a certain probability p. The dropout rate selected for this application is 5%, determined as the optimal value after conducting a parametric sweep. This makes the architecture less dependent on specific neurons and less prone to overfitting [51].

Adversarial training [57] has been used as another regularization technique. It consists of two networks, RUL regressor, and a cell classifier or Adversarial Network (AN). The AN is a classification network that has been connected to the outputs of the CNN (it has the same inputs as the feed-forward network), and as many outputs as battery cells in the dataset. During training, the CNN pre-processes the data and the feed-forward network obtains an estimate for RUL, while the AN classifies the specific cell the data comes from, to try to differentiate specific cell behaviours. The loss function for the RUL regressor is obtained as the mean squared error (MSE) between the estimate and the target RUL, while the loss function for the AN network is obtained as the cross-entropy loss between its output and the target cell. The overall loss function is composed as the loss function for the regressor minus the loss function of the classifier, multiplied by a certain factor λ, as in (4)

$$J = J_{MSE} - \lambda J_{CEL} \tag{4}$$

where J is the overall loss function value, J_{MSE} is the loss function for the RUL regressor, and J_{CEL} is the loss function for the AN. By training with this loss function, the regression network estimates RUL while, at the same time, the AN subnetwork avoids learning specific individual cell behaviours, thus limiting the overfitting capabilities.

All regularization-related hyperparameters and model design hyperparameters have been selected with the objective of optimizing performance, specifically targeting lower RUL prediction error. Throughout the model design process,

several parametric sweeps were conducted to find the better value for each hyperparameter for every model.

Regarding the final implementation of the RUL estimation model, the neural networks should be retrained with the whole dataset [58]. This way, all cells will be used for building the model. Notice that since there are only 124 cells available, any of them could provide meaningful information that would be omitted by using the standard cross-validation.

IV. RESULTS

The results achieved by using CNN and LSTM with the different approaches explained in Section II and Section III are collected in Table 3, including the details for each of the variations. In addition, results achieved by using other machine learning models found in the literature, are included. The Root Mean Square Error (RMSE) is used as evaluation metric:

$$RMSE = \sqrt{\sum_{i=1}^{n} \frac{\left(\hat{y}_i - y_i\right)^2}{n}} \tag{5}$$

where n is the number of examples in the test set, $\hat{y}_i$ is the predicted RUL for the i-th example, and y_i is the actual RUL value for the i-th example, measured in FEC.

TABLE 3. RMSE error metrics.

Model	RMSE (FECs)
CNN: IC waveforms only	156.9
CNN: Normalized IC waveforms	116.8
LSTM: IC waveforms only	96.3
LSTM: Normalized IC waveforms	93.3
Feed-Forward Net: Additional features only	93.4
CNN: IC + Additional features	75.6
LSTM: IC + Additional features	88.2
CNN: Ridge (λ = 0.003, k-CV training)	71.7
CNN: Lasso (λ = 0.003, k-CV training)	75.3
CNN: Dropout Layers (p = 5%, k-CV training)	85.3
CNN: Adversarial training (λ = 1, k-CV training)	75.7
CNN: Ridge (λ = 0.003, LOO training)	62.4
State of the art results by models proposed by other authors	
BL	115.9
ELM	105.6
BL-ELM	75.8

By analysing the first section of the table, it is worth noting that the version of the algorithm that includes normalized IC waveforms performs much better than the non-normalized version. By normalizing, the original shape of the waveforms is not preserved, and therefore some information is lost (the information of capacity is contained as the integral of the IC curve, and thus it is lost when normalizing these curves). However, it seems that the training process is easier due to the normalized data, and the algorithms perform better.

These results have been compared with those from a simple feed-forward network [51], that it is only trained with the additional features (capacity, IR, and TIEDVD). The error metrics achieved are comparable to those of more sophisticated algorithms which process IC curves. This suggests that both the IC waveforms and the additional variables provide relevant information for RUL estimation.

The next error metrics included in Table 3 belong to the CNN and LSTM algorithms, when information from IC waveforms and the additional variables are combined. As can be observed, when including the additional features, both algorithms perform much better, and the CNN provides clearly better results. At this point, we select the CNN as the winning architecture to apply the regularization techniques explained in Section III-B.

Among the different regularization techniques implemented, the best results were obtained when using Ridge regularization with $\lambda = 0{,}003$. When all these parameters are configured, the 10-fold cross-validation and LOO are performed, and the results in Table 3 show errors as low as 71.7 FECs and 62.4 FECs respectively.

Explainability is an important issue, but difficult to achieve in deep learning models. To provide more insight on how the CNN processes data and its automatic feature extraction capability, Fig. 7 show intermediate IC images (feature maps) produced by each CNN layer, for a new cell and for an aged cell. In the case of the new cell, only a single main peak is observed in the curves, that it is emphasized and propagated across the subsequent layers. In the case of the aged cell, it can be appreciated a secondary peak, and how the network amplifies and emphasizes it, to finally use both peaks as input for the post-processing network.

To compare our results with those of other state-of-the-art models, for instance, in [35] the authors use deep learning methods, such as auto-encoders, and classical methods, such as Bayesian Regression or SVM, resulting in a better performance of auto-encoders, but with a considerable error.

On the other hand, in [47] a similar estimation objective is pursued using a combination of Broad Learning (BL) and Extreme Learning Machine (ELM) applied to this dataset to predict RUL, by using the first test cycles of the cell. These results are collected in the last part of Table 3 for comparison. However, their approach differs from ours, since they use information from the first life of the cell, which is less suitable for a real second life application, where data from the previous life may not be available. As stated before, the main novelty of our methodology is that it does not require data from the cell's first life, and that only data from the ten laboratory cycles specifically performed to estimate RUL are used as inputs. The main conclusion is that the CNN shows similar error ranges in both cases, albeit ultimately lower, without using information from the past life of the battery in our case.

Finally, Table 4 shows the distribution of the output errors depending on the actual RUL region, corresponding to new, slightly used, heavily used, and aged cells. As expected, when predicting the remaining life of newer cells (higher RUL regions), the error is higher. In a realistic second life application scenario, cells under study will be aged cells and they will not be in these RUL ranges, so the lower accuracy of the algorithms in this region is not relevant. As cells approach

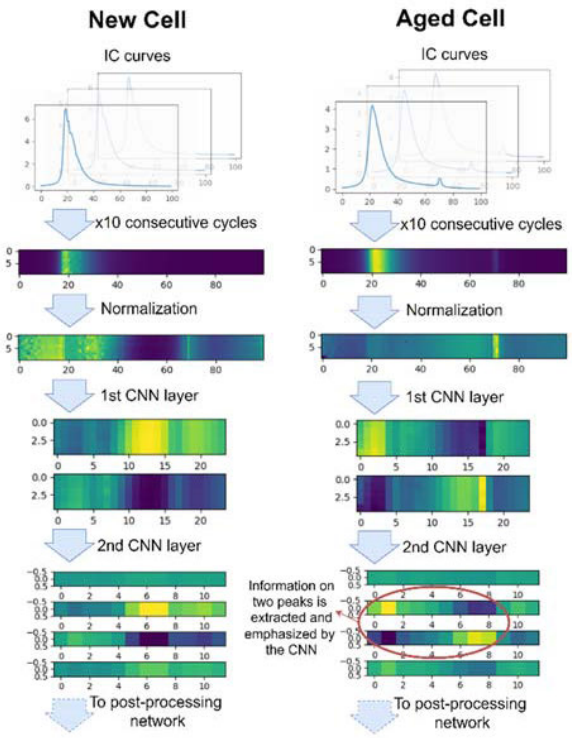

FIGURE 7. **Intermediate IC images (feature maps) produced by each CNN layer, for a new cell and for an aged cell, are shown. In the case of the aged cell, the secondary peak is detected, and the network amplifies and emphasizes it, until reaching the post processing net.**

their end of life (heavily used and aged cells), the predictions become more accurate, with consistent RMSE of 71.2 FECs for cells with actual RUL between 400 and 800 cycles, and down to 31.2 RMSE cycles for aged cells, with less than 400 remaining FEC.

TABLE 4. **RMSE in different RUL regions.**

Batteries	RUL regions (FECs)	RMSE (FECs)
New batteries	RUL >1200	252.3
Slightly used batteries	1200≥ RUL >800	128.5
Heavily used batteries	800≥ RUL >400	71.2
Aged batteries	400≥ RUL >0	31.2

V. CONCLUSION

This work addresses the estimation of RUL of lithium-ion batteries from a second life application point of view. Due to the complexity of the aging process of these cells, data-driven techniques are appropriate. These methods require datasets to be trained, they use knowledge (data) of the past usage of the cell to predict its behaviour. In this work, a publicly available dataset of 124 cells has been used, including 96,700 charge/discharge cycles, which has allowed us to arrange a set of 84,762 training examples.

One of the main novelties of our work is the estimation approach. In a real scenario, when a battery cell candidate for the second life market must be evaluated to estimate its RUL, information (data) on the first life of the cell is not available. Thus, in our work, data from only a few (ten) battery test cycles have been used to RUL prediction, contrary to most approaches in the literature, which require data of the whole battery lifespan.

The second main novelty of our work is the use of raw IC curves, to avoid the information loss associated with conventional manual feature extraction techniques. For processing the IC curves, several deep learning architectures, adequate for moderately sized datasets, have been trained and analysed, performing automatic feature extraction. The best results have been obtained with CNN models, processing a virtual image consisting of ten IC curves.

As indicated in Section III, we have been careful to obtain robust RUL estimation models, with good generalization capabilities despite the limited number of training examples, by using a broad set of regularization techniques. The best results have been achieved by using Ridge regularization and a LOO training process. An RMSE of only about 62 cycles on average for cells that live up to 1,200 cycles is achieved, lower than the error provided by state-of-the-art algorithms, which even make use of information on the first-life use. The results are especially good for deeply aged batteries (with less than 400 remaining FECs), where the RMSE goes down to about 31 cycles, an error of approximately 10%.

To provide more insight into the model operation, the evolution of the data through the CNN has been analysed. It has been observed how the CNN is able to detect and amplify the secondary IC peaks, which are key health indicators that provide useful information for RUL estimation.

As a final contribution, it has been made explicit the two levels of overfitting that can appear when working with this kind of datasets, where data is correlated on a cycle-level basis and a cell-level basis. Realizing that these two levels of overfitting is taking place is key to obtaining reliable results from data-driven algorithms, especially when using high-variance networks, which are prone to overfitting data.

As a future research line, the methodology presented in this paper is meant to be applied to more realistic datasets, with real application waveforms and with cells aged under different effects and mechanisms. This could be done by collecting data from realistic applications, or by using complex cell models to generate virtual datasets with different aging conditions. This virtualization could also evolve into an interesting research line by allowing the simulation of whole cell modules, thus creating module-level datasets aiming to expand the RUL estimation capabilities to more complex systems.

REFERENCES

[1] B. Nykvist and M. Nilsson, "Rapidly falling costs of battery packs for electric vehicles," *Nature Climate Change*, vol. 5, no. 4, pp. 329–332, Apr. 2015.

[2] B. Dunn, H. Kamath, and J.-M. Tarascon, "Electrical energy storage for the grid: A battery of choices," *Science*, vol. 334, no. 6058, pp. 928–935, Nov. 2011.

[3] B. Diouf and R. Pode, "Potential of lithium-ion batteries in renewable energy," *Renew. Energy*, vol. 76, pp. 375–380, Apr. 2015.

[4] S. B. Peterson, J. Apt, and J. F. Whitacre, "Lithium-ion battery cell degradation resulting from realistic vehicle and vehicle-to-grid utilization," *J. Power Sources*, vol. 195, no. 8, pp. 2385–2392, Apr. 2010.

[5] K. Young, C. Wang, L. Wang, and K. Strunz, "Electric vehicle battery technologies," in *Electric Vehicle Integration Into Modern Power Networks*. New York, NY, USA: Springer, 2013, pp. 15–56.

[6] C. Ioakimidis, A. Murillo-Marrodán, A. Bagheri, D. Thomas, and K. Genikomsakis, "Life cycle assessment of a lithium iron phosphate (LFP) electric vehicle battery in second life application scenarios," *Sustainability*, vol. 11, no. 9, p. 2527, May 2019.

[7] M. Farhadi and O. Mohammed, "Energy storage systems for high power applications," in *Proc. IEEE Ind. Appl. Soc. Annu. Meeting*, Oct. 2015, pp. 1–7.

[8] D. Ansean, M. Gonzalez, V. M. Garcıa, J. C. Viera, J. C. Anton, and C. Blanco, "Evaluation of $LiFePO_4$ batteries for electric vehicle applications," *IEEE Trans. Ind. Appl.*, vol. 51, no. 2, pp. 1855–1863, Jul. 2015.

[9] E. Martinez-Laserna, I. Gandiaga, E. Sarasketa-Zabala, J. Badeda, D.-I. Stroe, M. Swierczynski, and A. Goikoetxea, "Battery second life: Hype, hope or reality? A critical review of the state of the art," *Renew. Sustain. Energy Rev.*, vol. 93, pp. 701–718, Oct. 2018.

[10] R. Reinhardt, I. Christodoulou, S. Gassó-Domingo, and B. A. García, "Towards sustainable business models for electric vehicle battery second use: A critical review," *J. Environ. Manage.*, vol. 245, pp. 432–446, Sep. 2019.

[11] Y. Jiang, J. Jiang, C. Zhang, W. Zhang, Y. Gao, and N. Li, "State of health estimation of second-life LiFePO4 batteries for energy storage applications," *J. Cleaner Prod.*, vol. 205, pp. 754–762, Dec. 2018.

[12] E. Hossain, D. Murtaugh, J. Mody, H. M. R. Faruque, Md. S. Haque Sunny, and N. Mohammad, "A comprehensive review on second-life batteries: Current state, manufacturing considerations, applications, impacts, barriers & potential solutions, business strategies, and policies," *IEEE Access*, vol. 7, pp. 73215–73252, 2019.

[13] R. B. Wright, J. P. Christophersen, C. G. Motloch, J. R. Belt, C. D. Ho, V. S. Battaglia, J. A. Barnes, T. Q. Duong, and R. A. Sutula, "Power fade and capacity fade resulting from cycle-life testing of advanced technology development program lithium-ion batteries," *J. Power Sources*, vols. 119–121, pp. 865–869, Jun. 2003.

[14] M. Broussely, S. Herreyre, P. Biensan, P. Kasztejna, K. Nechev, and R. Staniewicz, "Aging mechanism in Li ion cells and calendar life predictions," *J. Power Sources*, vols. 97–98, pp. 13–21, May 2001.

[15] I. Bloom, B. W. Cole, J. J. Sohn, S. A. Jones, E. G. Polzin, V. S. Battaglia, G. L. Henriksen, C. Motloch, R. Richardson, T. Unkelhaeuser, D. Ingersoll, and H. L. Case, "An accelerated calendar and cycle life study of Li-ion cells," *J. Power Sources*, vol. 101, no. 2, pp. 238–247, Oct. 2001.

[16] H. Chaoui and C. C. Ibe-Ekeocha, "State of charge and state of health estimation for lithium batteries using recurrent neural networks," *IEEE Trans. Veh. Technol.*, vol. 66, no. 10, pp. 8773–8783, Oct. 2017.

[17] S. F. Schuster, T. Bach, E. Fleder, J. Müller, M. Brand, G. Sextl, and A. Jossen, "Nonlinear aging characteristics of lithium-ion cells under different operational conditions," *J. Energy Storage*, vol. 1, pp. 44–53, Jun. 2015.

[18] P. Pastor-Flores, B. Martín-del-Brío, A. Bono-Nuez, I. Sanz-Gorrachategui, and C. Bernal-Ruiz, "Unsupervised neural networks for identification of aging conditions in Li-ion batteries," *Electronics*, vol. 10, no. 18, p. 2294, Sep. 2021.

[19] D. Liu, W. Xie, H. Liao, and Y. Peng, "An integrated probabilistic approach to lithium-ion battery remaining useful life estimation," *IEEE Trans. Instrum. Meas.*, vol. 64, no. 3, pp. 660–670, Mar. 2015.

[20] L. Li, Y. Peng, Y. Song, and D. Liu, "Lithium-ion battery remaining useful life prognostics using data-driven deep learning algorithm," in *Proc. Prognostics Syst. Health Manage. Conf. (PHM-Chongqing)*, Oct. 2018, pp. 1094–1100.

[21] R. Khelif, B. Chebel-Morello, S. Malinowski, E. Laajili, F. Fnaiech, and N. Zerhouni, "Direct remaining useful life estimation based on support vector regression," *IEEE Trans. Ind. Electron.*, vol. 64, no. 3, pp. 2276–2285, Mar. 2017.

[22] D. Liu, H. Wang, Y. Peng, W. Xie, and H. Liao, "Satellite lithium-ion battery remaining cycle life prediction with novel indirect health indicator extraction," *Energies*, vol. 6, no. 8, pp. 3654–3668, Jul. 2013.

[23] C. Chen and M. Pecht, "Prognostics of lithium-ion batteries using model-based and data-driven methods," in *Proc. IEEE Prognostics Syst. Health Manage. Conf. (PHM- Beijing)*, May 2012, pp. 1–6.

[24] J. Liu and Z. Chen, "Remaining useful life prediction of lithium-ion batteries based on health indicator and Gaussian process regression model," *IEEE Access*, vol. 7, pp. 39474–39484, 2019.

[25] E. Martinez-Laserna, E. Sarasketa-Zabala, I. Villarreal Sarria, D.-I. Stroe, M. Swierczynski, A. Warnecke, J.-M. Timmermans, S. Goutam, N. Omar, and P. Rodriguez, "Technical viability of battery second life: A study from the ageing perspective," *IEEE Trans. Ind. Appl.*, vol. 54, no. 3, pp. 2703–2713, May 2018.

[26] D. Liu, Y. Luo, Y. Peng, X. Peng, and M. Pecht, "Lithium-ion battery remaining useful life estimation based on nonlinear AR model combined with degradation feature," in *Proc. Annu. Conf. Prognostics Health Manage. Soc.*, vol. 9, 2012, pp. 1–7.

[27] D. Z. Li, W. Wang, and F. Ismail, "A mutated particle filter technique for system state estimation and battery life prediction," *IEEE Trans. Instrum. Meas.*, vol. 63, no. 8, pp. 2034–2043, Aug. 2014.

[28] D. Wang, F. Yang, K.-L. Tsui, Q. Zhou, and S. J. Bae, "Remaining useful life prediction of lithium-ion batteries based on spherical cubature particle filter," *IEEE Trans. Instrum. Meas.*, vol. 65, no. 6, pp. 1282–1291, Jun. 2016.

[29] Z. Liu, G. Sun, S. Bu, J. Han, X. Tang, and M. Pecht, "Particle learning framework for estimating the remaining useful life of lithium-ion batteries," *IEEE Trans. Instrum. Meas.*, vol. 66, no. 2, pp. 280–293, Feb. 2017.

[30] W. Zhang, X. Li, and X. Li, "Deep learning-based prognostic approach for lithium-ion batteries with adaptive time-series prediction and on-line validation," *Measurement*, vol. 164, Nov. 2020, Art. no. 108052.

[31] M. Dubarry, G. Baure, and D. Anseán, "Perspective on state-of-health determination in lithium-ion batteries," *J. Electrochemical Energy Convers. Storage*, vol. 17, no. 4, Nov. 2020, Art. no. 044701, doi: 10.1115/1.4045008.

[32] K. Luo, X. Chen, H. Zheng, and Z. Shi, "A review of deep learning approach to predicting the state of health and state of charge of lithium-ion batteries," *J. Energy Chem.*, vol. 74, pp. 159–173, Nov. 2022, doi: 10.1016/j.jechem.2022.06.049.

[33] X. Li, D. Yu, V. Søren Byg, and S. D. Ioan, "The development of machine learning-based remaining useful life prediction for lithium-ion batteries," *J. Energy Chem.*, vol. 82, pp. 103–121, Jul. 2023.

[34] L. Ren, L. Zhao, S. Hong, S. Zhao, H. Wang, and L. Zhang, "Remaining useful life prediction for lithium-ion battery: A deep learning approach," *IEEE Access*, vol. 6, pp. 50587–50598, 2018.

[35] K. A. Severson, P. M. Attia, N. Jin, N. Perkins, B. Jiang, Z. Yang, M. H. Chen, M. Aykol, P. K. Herring, D. Fraggedakis, M. Z. Bazant, S. J. Harris, W. C. Chueh, and R. D. Braatz, "Data-driven prediction of battery cycle life before capacity degradation," *Nature Energy*, vol. 4, no. 5, pp. 383–391, Mar. 2019.

[36] D. Chen, W. Hong, and X. Zhou, "Transformer network for remaining useful life prediction of lithium-ion batteries," *IEEE Access*, vol. 10, pp. 19621–19628, 2022, doi: 10.1109/ACCESS.2022.3151975.

[37] X. Gu, K. W. See, P. Li, K. Shan, Y. Wang, L. Zhao, K. C. Lim, and N. Zhang, "A novel state-of-health estimation for the lithium-ion battery using a convolutional neural network and transformer model," *Energy*, vol. 262, Jan. 2023, Art. no. 125501.

[38] N. Costa, D. Anseán, M. Dubarry, and L. Sánchez, "ICFormer: A deep learning model for informed lithium-ion battery diagnosis and early knee detection," *J. Power Sources*, vol. 592, Feb. 2024, Art. no. 233910.

[39] M. Dubarry, V. Svoboda, R. Hwu, and B. Yann Liaw, "Incremental capacity analysis and close-to-equilibrium OCV measurements to quantify capacity fade in commercial rechargeable lithium batteries," *Electrochem. Solid-State Lett.*, vol. 9, no. 10, p. A454, 2006.

[40] M. Berecibar, M. Dubarry, N. Omar, I. Villarreal, and J. Van Mierlo, "Degradation mechanism detection for NMC batteries based on incremental capacity curves," *World Electr. Vehicle J.*, vol. 8, no. 2, pp. 350–361, Jun. 2016.

[41] D. Anseán, M. González, C. Blanco, J. C. Viera, Y. Fernández, and V. M. García, "Lithium-ion battery degradation indicators via incremental capacity analysis," in *Proc. IEEE Int. Conf. Environ. Electr. Eng. IEEE Ind. Commercial Power Syst. Eur.*, At Milan, Italy, Jun. 2017, pp. 1–6.

[42] L. Li, Y. Zhu, L. Wang, D. Yue, and D. Li, "Indirect remaining useful life prognostics for lithium-ion batteries," in *Proc. 24th Int. Conf. Autom. Comput. (ICAC)*, Sep. 2018, pp. 1–5.

[43] E. Schaltz, D.-I. Stroe, K. Nørregaard, L. S. Ingvardsen, and A. Christensen, "Incremental capacity analysis applied on electric vehicles for battery state-of-health estimation," *IEEE Trans. Ind. Appl.*, vol. 57, no. 2, pp. 1810–1817, Mar. 2021, doi: 10.1109/TIA.2021.3052454.
[44] D.-I. Stroe and E. Schaltz, "Lithium-ion battery state-of-health estimation using the incremental capacity analysis technique," *IEEE Trans. Ind. Appl.*, vol. 56, no. 1, pp. 678–685, Jan. 2020, doi: 10.1109/TIA.2019.2955396.
[45] N. Costa, L. Sánchez, D. Anseán, and M. Dubarry, "Li-ion battery degradation modes diagnosis via convolutional neural networks," *J. Energy Storage*, vol. 55, Nov. 2022, Art. no. 105558.
[46] P. Fermín-Cueto, E. McTurk, M. Allerhand, E. Medina-Lopez, M. F. Anjos, J. Sylvester, and G. dos Reis, "Identification and machine learning prediction of knee-point and knee-onset in capacity degradation curves of lithium-ion cells," *Energy AI*, vol. 1, Aug. 2020, Art. no. 100006.
[47] Y. Ma, L. Wu, Y. Guan, and Z. Peng, "The capacity estimation and cycle life prediction of lithium-ion batteries using a new broad extreme learning machine approach," *J. Power Sources*, vol. 476, Nov. 2020, Art. no. 228581.
[48] I. Sanz-Gorrachategui, P. Pastor-Flores, M. Pajovic, Y. Wang, P. V. Orlik, C. Bernal-Ruiz, A. Bono-Nuez, and J. S. Artal-Sevil, "Remaining useful life estimation for LFP cells in second-life applications," *IEEE Trans. Instrum. Meas.*, vol. 70, pp. 1–10, 2021.
[49] Q. Zhao, X. Qin, H. Zhao, and W. Feng, "A novel prediction method based on the support vector regression for the remaining useful life of lithium-ion batteries," *Microelectron. Rel.*, vol. 85, pp. 99–108, Jun. 2018.
[50] D. Liu, X. Yin, Y. Song, W. Liu, and Y. Peng, "An on-line state of health estimation of lithium-ion battery using unscented particle filter," *IEEE Access*, vol. 6, pp. 40990–41001, 2018.
[51] I. Goodfellow, Y. Bengio, and A. Courville, *Deep Learning*. Cambridge, MA, USA: MIT Press, 2016.
[52] S. J. Prince, *Understanding Deep Learning*. Cambridge, MA, USA: MIT Press, 2023.
[53] V. J. Lawhern, A. J. Solon, N. R. Waytowich, S. M. Gordon, C. P. Hung, and B. J. Lance, "EEGNet: A compact convolutional neural network for EEG-based brain–computer interfaces," *J. Neural Eng.*, vol. 15, no. 5, Jul. 2018, Art. no. 056013.
[54] S. Hochreiter and J. Schmidhuber, "Long short-term memory," *Neural Comput.*, vol. 9, no. 8, pp. 1735–1780, Nov. 1997.
[55] R. Kohavi, "A study of cross-validation and bootstrap for accuracy estimation and model selection," in *Proc. 14th Int. Joint Conf. Artif. Intell.*, 1995, no. 12, pp. 1137–1143.
[56] I. J. Goodfellow, J. Pouget-Abadie, M. Mirza, B. Xu, D. Warde-Farley, S. Ozair, A. Courville, and Y. Bengio, "Generative adversarial networks," in *Proc. Adv. Neural Inf. Process. Syst.*, vol. 27, 2014, pp. 1–5.
[57] Y. Ganin and V. Lempitsky, "Unsupervised domain adaptation by backpropagation," in *Proc. Int. Conf. Mach. Learn.*, 2015, pp. 1–5.
[58] Y. S. Abu-Mostafa, M. Magdon-Ismail, and H.-T. Lin, *Learning From Data*. New York, NY, USA:AMLBook, 2012.

I. SANZ-GORRACHATEGUI received the B.Sc. and M.Sc. degrees in communication and electrical engineering from the University of Zaragoza, Zaragoza, Spain, in 2015 and 2016, respectively, and the Ph.D. degree in electrical engineering from the Power Electronics and Micro-Electronics Group, Said University in 2021.

From 2019 to 2020, he was a Fulbright Scholar with the Mitsubishi Electric Research Laboratories, Cambridge, MA, USA. His current research interests include battery management systems architectures, SoX estimation techniques, and automated validation frameworks for BMS design.

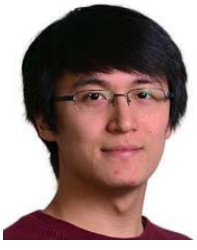

Y. WANG (Senior Member, IEEE) received the B.S. degree in electrical and computer engineering from Worcester Polytechnic Institute, in 2005, and the M.S. and Ph.D. degrees in electrical and computer engineering from Boston University, in 2009 and 2011, respectively. In 2012, he joined the Mitsubishi Electric Research Laboratories, where he has also previously completed an internship, in 2010. His research interests include information theory, machine learning, signal processing, communications, and data privacy/security.

A. GUILLÉN-ASENSIO received the B.Sc. and M.Sc. degrees in electrical engineering from the University of Zaragoza, Spain, in 2017 and 2019 respectively. He is currently a Researcher in machine learning techniques applied to energy systems. His research interests include predictive algorithms, energy storage systems, and battery modeling.

A. BONO-NUEZ received the M.Sc. and Ph.D. degrees in electronic engineering from the University of Zaragoza, Spain, in 2008 and 2016, respectively. Since 2001, he has been with the University of Zaragoza, as an Adjunct Professor and a Lecturer of electronic engineering. He is the author of two patents and more than 40 papers and congress communications. His main research interest includes machine learning applied to energy storage systems and its implementation.

B. MARTÍN-DEL-BRÍO (Senior Member, IEEE) received the Ph.D. degree (Hons.), in 1994. He is an Associate Professor of electronics engineering with the University of Zaragoza, Spain. He has made research stays at Madrid and Sweden. He has authored two textbooks, over 100 papers and congress communications, and holds two patents. His main research interests include smart sensing and machine learning.

P. V. ORLIK (Senior Member, IEEE) received the B.E., M.S., and Ph.D. degrees in electrical engineering from the State University of New York (SUNY) at Stony Brook, Stony Brook, NY, USA, in 1994, 1997, and 1999, respectively.

From 1999 to 2000, he was a Simulation and Modeling Engineer with Mitre Corporation, McLean, VA, USA. In 2000, he joined Mitsubishi Electric Research Laboratories (MERL) Inc., Cambridge, MA, USA, as a member of Technical Staff. He is currently the Manager of the Signal Processing Group. His current research interests include advanced signal processing methods for various applications, including radar, material sensing, advanced wireless and wired communications, sensor, and the Internet of Things (IoT) networks. Other research interests include vehicular/car-to-car communications, mobility modeling, performance analysis, and queuing theory.

P. PASTOR-FLORES received the B.Sc. and M.Sc. degrees in electrical engineering from the University of Zaragoza, Spain, in 2018 and 2019 respectively, where he is currently pursuing the Ph.D. degree in machine learning techniques applied to energy systems. His research interests include unsupervised learning, SOH algorithms, and battery aging.